arXiv:1510.04344v1 [cond-mat.quant-gas] 14 Oct 2015

Robust Vortex Lines, Vortex Rings and Hopfions in 3D Bose-Einstein Condensates

R.N. Bisset,[1,*] Wenlong Wang,[2] C. Ticknor,[3] R. Carretero-González,[4]
D.J. Frantzeskakis,[5] L.A. Collins,[3] and P.G. Kevrekidis[6,1]

[1] *Center for Nonlinear Studies and Theoretical Division, Los Alamos National Laboratory, Los Alamos, NM 87545*
[2] *Department of Physics, University of Massachusetts, Amherst, Massachusetts 01003 USA*
[3] *Theoretical Division, Los Alamos National Laboratory, Los Alamos, NM 87545*
[4] *Nonlinear Dynamical Systems Group, Computational Sciences Research Center, and Department of Mathematics and Statistics, San Diego State University, San Diego, California 92182-7720, USA*
[5] *Department of Physics, University of Athens, Panepistimiopolis, Zografos, Athens 15784, Greece*
[6] *Department of Mathematics and Statistics, University of Massachusetts, Amherst, Massachusetts 01003-4515 USA*

(Dated: October 16, 2015)

Performing a systematic Bogoliubov-de Gennes spectral analysis, we illustrate that stationary vortex lines, vortex rings and more exotic states, such as hopfions, are robust in three-dimensional atomic Bose-Einstein condensates, for large parameter intervals. Importantly, we find that the hopfion can be stabilized in a simple parabolic trap, without the need for trap rotation or inhomogeneous interactions. We supplement our spectral analysis by studying the dynamics of such stationary states; we find them to be robust against significant perturbations of the initial state. In the unstable regimes, we not only identify the unstable mode, such as a quadrupolar or hexapolar mode, but we also observe the corresponding instability dynamics. Furthermore, deep in the Thomas-Fermi regime, we investigate the particle-like behavior of vortex rings and hopfions.

Introduction: Atomic Bose-Einstein condensates (BECs) have offered, over the last two decades, a fertile playground for the exploration of nonlinear matter waves [1–3]. While a large volume of the early work along this vein focused on solitons and vortices, the remarkable advancement of computational resources has rendered more accessible the frontier of three-dimensional (3D) structures. Arguably, the most prototypical among the latter, not only in superfluid but also in regular fluid settings [4, 5], is the vortex ring (VR). VRs have not only been theoretically predicted, but also experimentally observed (see the reviews [3, 6, 7]).

In addition to the VRs and vortex lines (VLs) extensively studied in earlier BEC experiments (see, e.g., Refs. [8, 9] and a more recent experimental realization in Ref. [10]), BECs may support more complex topological structures, such as Skyrmions in multi-component settings. In its simplest realization, originally proposed in Refs. [11, 12], the Skyrmion consisted of a VR in one-component, coupled to a VL in the second component. Interestingly, more complex Skyrmion states involving three-component spinor BECs were realized experimentally in both two- [13] and three-dimensions [14], involving respectively, coupled states of topological charge $S = -1, 0, 1$ and $S = 0, 1, 2$, and described in the recent theoretical work of Ref. [15]. Of increasing interest of late is the one-component counterpart to the Skyrmion, namely the so-called hopfion state [16, 17]. This state consists of a VR and VL in the same component, with the axis of the VR coinciding with that of the VL. A stable hopfion state has so far only been predicted in somewhat complicated experimental configurations. These include, for instance, elaborated radially increasing nonlinear interactions [16], or a rotation of the trap [17]. Here we show that the hopfion can, in fact, be stable for large chemical potential ranges and simple trapping configurations, i.e., inside a parabolic trap.

Our main aim is to provide a systematic stability analysis of VRs, hopfions and, in passing, VLs. By a detailed understanding of the pertinent modes of the Bogoliubov-de Gennes (BdG) linearization, we are able to explain when the relevant stationary states are stable or unstable. We also elucidate, both, how such properties depend on geometric characteristics such as the trap aspect ratio, and what instabilities one may encounter in different parameter intervals. These results should pave the way for the experimental identification of such coherent structures in state-of-the-art experimental setups of 3D BECs.

In what follows, we first discuss the stability properties of the VR from an analytical perspective. We then corroborate these analytical predictions of the relevant modes by means of highly-intensive numerical spectrum computations. We also show how the stability of the VR and the VL implies the potential stability of the hopfion pattern, and confirm this with our numerics. Finally, we provide an exploration of the unstable dynamics of the VR and hopfion states informed by both spectral properties and direct numerical simulations.

Analytical Considerations: We begin with the 3D Gross-Pitaevskii equation (GPE):

$$i\psi_t = -\frac{\hbar^2}{2m}\nabla^2\psi + V(r)\psi + g|\psi|^2\psi, \qquad (1)$$

where ψ is the wavefunction of the 3D Bose-gas near zero temperature, $g = 4\pi\hbar^2 a_s/m$, with a_s being the s-wave scattering length and m is the particle mass. The potential assumes the prototypical form of the harmonic

oscillator, $V(x,y,z) = m\omega_r^2 r^2/2 + m\omega_z^2 z^2/2$, with ω_r and ω_z being the planar and transverse trapping strengths, respectively. The case of $\omega_z > \omega_r$ leads to an oblate BEC, while the reverse inequality produces a prolate BEC.

In earlier work we explored the bifurcation of a VR near the linear limit of low density, either from a planar or from a ring dark soliton [18]; here, our focus will be on the opposite limit. In particular, we consider the case of large chemical potential (and small healing length) where the VRs can be considered as particle-like objects in their behavior and dynamics. Reference [19], following the pioneering work of Ref. [20], explored the dynamics of the single VR in the presence of a trap. This is also examined in Ref. [21], where the results of Ref. [19] are utilized. In particular, in Ref. [19], the expression for the velocity of a vortex line element is given by

$$\mathbf{v}(\mathbf{x}) = \Lambda \left(\kappa \hat{\mathbf{b}} + \frac{\hat{\mathbf{t}} \times \nabla V}{F(r,z)} \right), \tag{2}$$

where $\Lambda = (-1/2)\ln(\sqrt{R_r^{-2} + \kappa^2/8}/\sqrt{2\mu})$ and κ denotes the curvature of the element (for a VR $\kappa = 1/r$). We denote by $\hat{\mathbf{b}}$ the binormal vector (for the axisymmetric VR, it is $\hat{\mathbf{z}}$), while $\hat{\mathbf{t}}$ denotes the tangent vector (equal to $\hat{\theta}$ for the VR). The quantity $F(r,z) = \max\{\mu - V(r), 0\}$, represents the Thomas-Fermi (TF) density profile, relevant to the case of large density, equivalent to large chemical potential, analyzed here; the corresponding radial and axial TF radii are given by $R_{r,z} = (2\mu/\omega_{r,z}^2)^{1/2}$. Note that Λ is accurate up to logarithmic corrections, which will be responsible for the approximate nature of the analytical results (in comparison to the numerical findings) in what follows.

Assuming that $\Lambda(r)$ varies slowly with r (indeed logarithmically), the following equations of motion are then derived for a single VR inside the trap [21]:

$$\frac{1}{\Lambda(r)}\dot{r} = \frac{\omega_z^2 z}{F(r,z)}, \quad \dot{\theta} = 0, \quad \frac{1}{\Lambda(r)}\dot{z} = \frac{-\omega_r^2 r}{F(r,z)} + \frac{1}{r}. \tag{3}$$

These equations predict the presence of an equilibrium radius of the VR in the $z = 0$ plane, i.e. $r_{\rm eq} = \sqrt{2\mu/(3\omega_r^2)}$. This effective radius seems to provide a natural generalization of the radius of the ring dark soliton [22, 23], and is also in line with earlier results [24].

Reference [21] chiefly focused on considering the dynamics of azimuthal perturbations (Kelvin-wave type modulations) using Eq. (2). In particular, they linearized around the stationary solution $(r,z) = (r_{\rm eq}, 0)$, using a perturbation of the form $r(t) = r_{\rm eq} + R_1(t)e^{in\phi}$ and $z(t) = Z_1 e^{in\phi}$, for integer n. Substitution of this linearization ansatz in Eq. (2) provides a generalized set of equations [Eqs. (5) and (6) in Ref. [21]] from which the effect of the azimuthal modulations on the motion of the VR can also be evaluated. Importantly, notice that this set of equations can account for the $n = 0$ oscillatory motion of the VR inside the trap, described by Eq. (3). The final result that we explore numerically in what follows is that the frequencies of vibration of the VR are given by,

$$\omega = \pm \frac{3\Lambda(r_{\rm eq})\omega_r^2}{2\mu} \left[(n^2 - \frac{\omega_z^2}{\omega_r^2})(n^2 - 3) \right]^{1/2}. \tag{4}$$

Importantly, we intend to test the ensuing implication that the VR stability depends on the shape of the condensate. More specifically, if the condensate is prolate ($\omega_z/\omega_r < 1$), then the VR should be unstable due to the $n = 1$ mode. If the condensate is spherical to slightly oblate ($1 \leq \omega_z/\omega_r \leq 2$), then at the particle level and under azimuthal perturbations, the VR and VL should be stable. Finally, for sufficiently oblate condensates, with $\omega_z/\omega_r > 2$, the VR should be unstable due to the $n = 2, \ldots, [\omega_z/\omega_r]$ modes, where the brackets denote the integer part function.

Numerical Results: We start by considering the spectral linearization analysis around a VR state. The relevant BdG ansatz will be of the form:

$$\psi = e^{-i\mu t} \left[\psi_0 + \epsilon \left(u(x,y,z)e^{i\omega t} + v^*(x,y,z)e^{-i\omega^* t} \right) \right], \tag{5}$$

where μ is the chemical potential, the asterisks denotes complex conjugation, ϵ is a formal small parameter, and the presence of imaginary (or complex) eigenfrequencies ω reflects an instability along the direction of the corresponding eigenvector $(u,v)^T$.

In practice, we solve the GPE, Eq. (1), using a Newton-Krylov scheme [25]. For the BdG equations we utilize the azimuthal symmetry of the trap in a way similar to Refs. [26, 27]. This amounts to using spectral-basis modes that each have a definite angular momentum quantum number, m, proportional to $e^{im\phi}$. This way, we can treat the azimuthal variable analytically, effectively reducing the problem to 2D. Importantly, for a given excitation, the coupling between m-subspaces is limited, and this allows the diagonalization of relatively small subsets independently. Specifically, if the v of Eq. (5) resides in subspace m, then the u resides in subspace $m + 2s$, where s is the charge (angular momentum quantum number) of the stationary state [28].

Our fundamental premise in what follows is that for the large μ regime, the spectrum of a state such as the VR or the VL consists of the union of two principal ingredients: the modes of vibration (undulation) of the VR or VL itself, and the modes of the underlying "ground state" (see Fig. 5 in the Supplemental Material), i.e., the TF cloud. The TF spectrum in this limit has been identified early on [30] and the internal modes of the VR are described by Eq. (4). Hence, in the numerical BdG spectra of Fig. 1(a) for $\omega_z/\omega_r = 1$ and Fig. 1(b) for $\omega_z/\omega_r = 2.8$, we expect to observe this union of modes. We find that this expectation is indeed confirmed in both of these figures. The TF vibrational modes predicted by Ref. [30] correspond to the constant frequencies (thin horizontal lines)

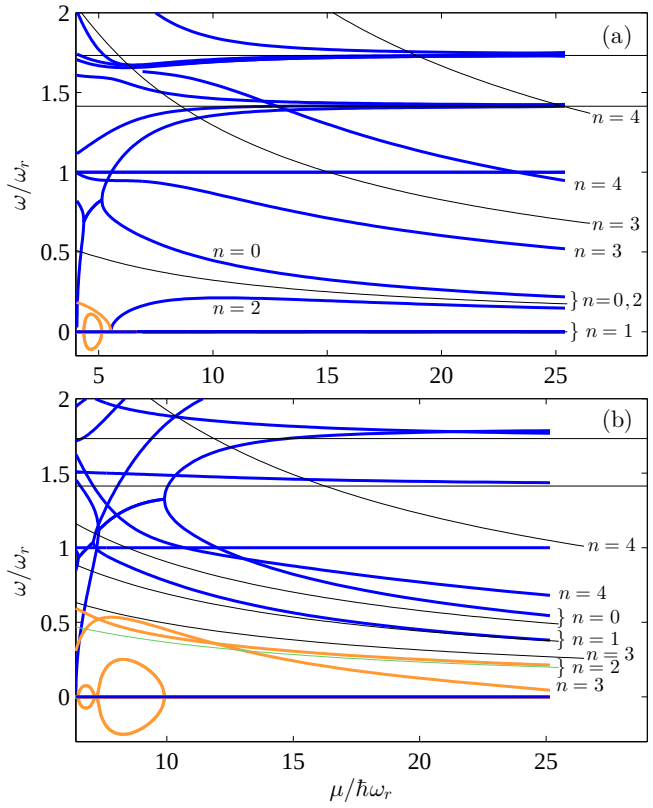

FIG. 1: (Color online) BdG-frequency spectrum for the vortex ring when (a) $\omega_z/\omega_r = 1$ and (b) $\omega_z/\omega_r = 2.8$. Stable (real) components are depicted by the thick blue (dark) lines and unstable (imaginary) components by the thick orange (light) lines. Thin lines are TF analytic predictions [black (dark) corresponding to real and green (light) to imaginary components of the eigenvalues] for the vortex ring [thin curved lines, Eq. (4)] and the ground state (thin horizontal lines; see Ref. [30]). The undulation number n [see Eq. (4)] of each excitation is indicated. For both geometries, the analytical prediction is in good agreement with the numerics for $n = 0, 1$ and 2, but deteriorates for $n > 2$.

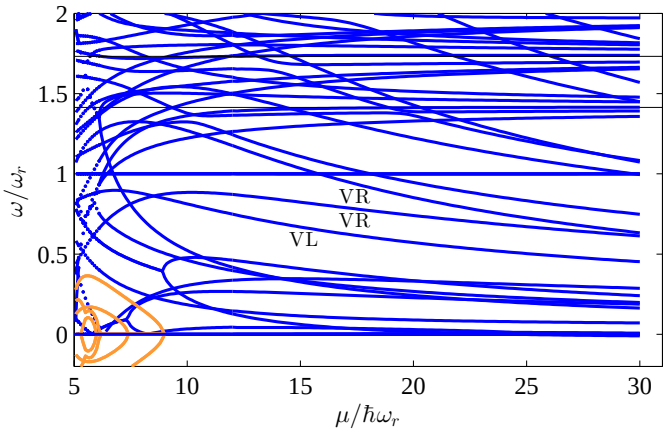

FIG. 2: (Color online) The spectrum of the hopfion with $\omega_z/\omega_r = 1$. The different types of curves have the same meaning as in Fig. 1. Importantly, we predict that the hopfion is stable for $\mu > 9$. While some excitations can be identified as strictly belonging to either the VR or the VL, see labeled examples, other excitations correspond to hybrid modes due to the coupling between the VR and the VL.

to which the relevant spectral modes approach asymptotically. On the other hand, the modes predicted by Eq. (4) feature a decay as $1/\mu$ (modulated by a logarithmic dependence). For the internal VR modes, the theoretical predictions, given by thin curved lines, reasonably approximate the numerical results, especially for larger values of μ. This approximation is especially good for the anomalous-vibration mode of the entire VR as a whole inside the trap ($n = 0$), as well as for undulations of the VR such as the dipolar ($n = 1$) and quadrupolar ($n = 2$) modes. We note, however, that for higher-order modes (larger values of n), the analytical prediction of their frequency, based on Eq. (4), is less accurate. The case of $\omega_z/\omega_r = 1$ is expected to be stable in the large μ limit, as predicted by Eq. (4), and indeed this is supported by our BdG analysis in Fig. 1(a). On the other hand, for $\omega_z/\omega_r = 2.8$, our results confirm that the VR is unstable due to the mode of $n = 2$, as was predicted by Eq. (4) — see Fig. 1(b). However, the mode of $n = 3$ is predicted to be stable analytically, while it is found to be unstable numerically, illustrating the limitations of the analytical prediction for $n > 2$.

Similar results can be found for the VL case (see Fig. 6 in the Supplemental Material). In this case, the analytical predictions could be suitably extended by taking the curvature to be 0, and accounting for $F(r, z)$ in Eq. (2) not being a constant. A nontrivial difference between the latter and the former case is that the VL is found to be generically stable for the isotropic limit of $\omega_z/\omega_r = 1$, i.e., the intervals of instability due to imaginary or complex eigenvalues observed in Fig. 1 are absent. The VR on the other hand features, for small μ, the unstable modes described in detail in Ref. [18].

Having identified stable VR and VLs in the isotropic limit for large μ suggests that the hopfion itself, consisting of a combined VR and VL in the same BEC, is likely to be stable in the TF limit. We have tested this prediction for $\omega_z/\omega_r = 1$ in Fig. 2: indeed, we observe that although instabilities may arise for small values of μ, for large values of μ the hopfion is robust. By investigation of the individual BdG eigenvectors we find that the spectrum encompasses the union of VR, VL and TF modes, with the analytical prediction for the latter [30] shown as thin horizontal lines. We have also labeled a few examples of purely VR and VL modes. However, we note that other modes demonstrate coupling between the VR and VL, as evidenced also by the hybrid nature of their BdG eigenvectors.

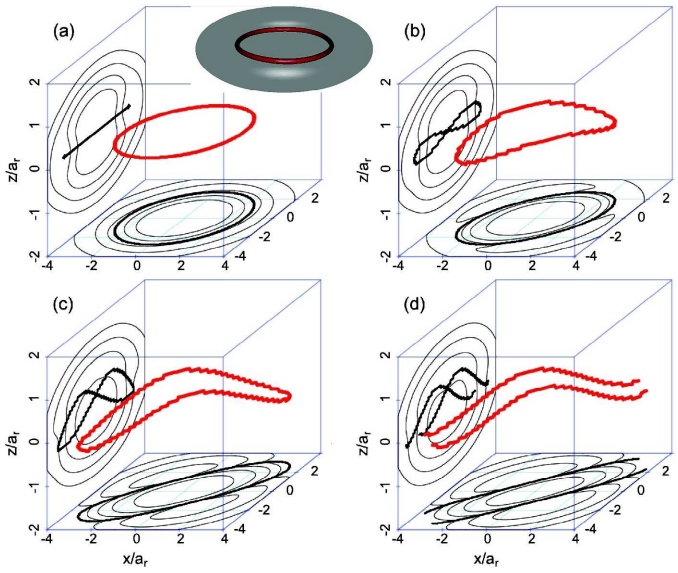

FIG. 3: (Color online) Dynamics of the VR, demonstrating instability to an $n = 2$ undulation, shown at times $\omega_r t = 3.5$ (a), 25.4 (b), 29.0 (c) and 30.0 (d). Parameters: $\omega_z/\omega_r = 2.8$ and $\mu/\hbar\omega_r \approx 15.3$. Red (gray) curves indicate vortex-core positions; thick black lines line show the vortex-core projections onto the (x, y) and (y, z) planes; thin-black contour lines represent the column density projections at 0.2, 0.4, 0.6 and 0.8 of the peak. Inset: iso-density surface of the stationary state at 0.1 of the peak; the inner iso-density surface of the VR is colored red. Units are that of the harmonic oscillator $a_r = \sqrt{\hbar/m\omega_r}$. To see a movie of the dynamics see Ref. [35] [Movie#1].

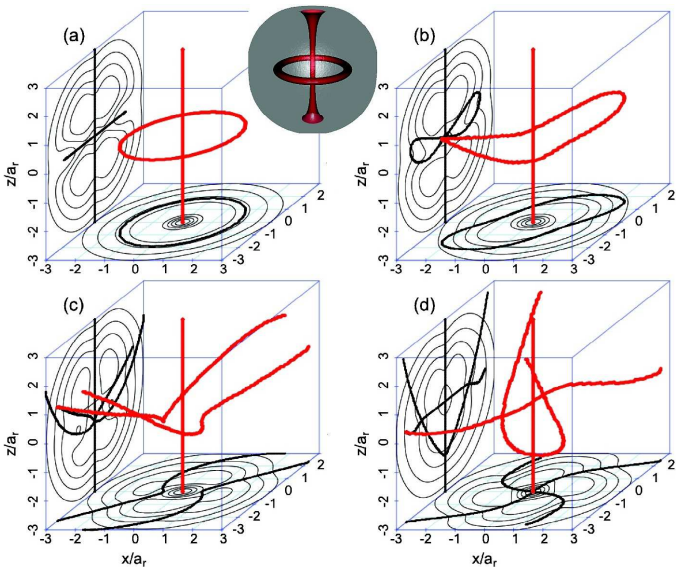

FIG. 4: (Color online) Dynamics of a hopfion instability at times $\omega_r t = 0$ (a), 40.9 (b), 42.4 (c) and 44.3 (d), after a random-noise seeding at $\omega_r t = 0$. Parameters: $\omega_z/\omega_r = 1$ and $\mu/\hbar\omega_r \approx 7.0$. Curves and contours have the same meanings as in Fig. 3. To see a movie of the dynamics see Ref. [35] [Movie#3].

To complement our spectral analysis, we explore the nonlinear dynamics of the VR and the hopfion, utilizing two methods. In the first, we temporally propagate the time-dependent GPE by employing a real-space product scheme, based on a split-operator approach, with the spatial component treated with a finite-element discrete-variable representation, using a Gauss-Legendre quadrature within each element [29]. For the second method, we use a split-step operator on an FFT grid. For the results presented herein, we find quantitative agreement between these two numerical methods.

We first discuss the stability of the hopfion. At $\mu = 12$, where according to Fig. 2 the hopfion is stable, we performed two stability tests. In the first, we added an average of 1% random noise to ψ_0 on each grid point at time $\omega_r t = 0$, and found that the hopfion remains robust for the entire duration of the test, up to time $\omega_r t = 200$. In the second test, we excited the hopfion by adding a special excitation ψ_1 at the 5% level, i.e. $\psi_0 \to \psi_0 + 0.05\psi_1$, and found the hopfion to undulate in a stable manner for more than $\omega_r t = 200$ time units. Note that ψ_1 is the most unstable mode for small chemical potentials, $\mu/\hbar\omega_r < 9$ (see Fig. 2).

We now consider the instability dynamics. In Fig. 3, we examine the dynamics of the VR in a regime where it is found to be dynamically unstable in our earlier spectral analysis, in particular due to the $n = 2$ quadrupolar mode. As a result, we observe that the relevant mode (i.e., the Kelvin wave) is amplified, until it eventually gives rise to the "rupture" of the VR into a pair of VLs. We have also observed similar dynamical evolutions where the instability is seeded by the unstable $n = 3$ mode (see Fig. 7 in the Supplemental Material). In this case, we found that the VR breaks into 6 VLs, before exhibiting a temporary revival of a smaller VR.

Finally, we examine the dynamical instability of the hopfion for $\mu \approx 7$, where it is still dynamically unstable prior to its stabilization for larger μ. The initial stages of the hopfion instability proceed in a similar manner to that of the VR. First, the VR part of the hopfion bends and then breaks into two VLs. The main difference arises when these VLs are subsequently pulled inwards to reconnect with the vertical VL. Interestingly, the VLs remain connected, with a '+' junction, for extended periods [see Fig.4(d)]. Note that such reconnection events, particularly interesting in their own right and especially relevant in turbulent dynamics (see, e.g., Refs. [31, 32]), have also been observed in the presence of rotation [17].

It is important to point out that the regimes considered in this work are experimentally accessible: for $\mu/\hbar\omega_r = 10.1$, a regime in which Fig. 2 predicts the hopfion to be stable, corresponds to a ^{87}Rb BEC containing $\approx 1.1\times10^4$ atoms in an isotropic trap with $\omega_z = \omega_r = 2\pi \times 50$ Hz.

Conclusions and Outlook. In the present work, we investigated 3D states that are supported in isotropic (and anisotropic) BECs. We used highly intensive numerical computations to explore their spectral stability, and found that, in the isotropic limit, the vortex line, vortex ring and their combined state, the hopfion, are dynamically stable in a wide parameter regime. Importantly, we predict the hopfion to be robust in "ordinary" condensates, within typical parameter regimes of a highly accessible parabolic trap. Not only did we identify this stability, but we provided a road map on how to "read" the spectrum of these different states and what principal ingredients are contained therein. Both the analytical approach and the numerical computations explained why different trap aspect ratios may drastically affect the stability properties of such states. Finally, when the states were deemed to be unstable, direct numerical simulations elucidated their breakup and subsequent dynamics, such as the vortex line reconnections in the case of the hopfion.

An interesting future direction would be the extension of our investigations to a higher number of components: in particular, in the two-component setting, the analogue of the hopfion would correspond to a Skyrmion, whose spectral and dynamical properties would be directly accessible through our approach. It would also be of interest to explore extensions in open systems, such as finite temperature BECs [33], the (chiefly quasi-two-dimensional) polariton superfluids [34], and damped-driven systems, more generally.

We thank A.J. White for useful discussions. W.W. acknowledges support from NSF (grant No. DMR-1208046). P.G.K. gratefully acknowledges the support of NSF-DMS-1312856, of the ERC under FP7, Marie Curie Actions, People, International Research Staff Exchange Scheme (IRSES-605096) and insightful discussions with Profs. I. Danaila and B. Malomed. R.C.G. gratefully acknowledges the support of NSF-DMS-1309035. The work of D.J.F. was partially supported by the Special Account for Research Grants of the University of Athens. This work was performed under the auspices of the Los Alamos National Laboratory, which is operated by LANS, LLC for the NNSA of the U.S. DOE under Contract No. DE-AC52-06NA25396.

* Electronic address: rnbisset@gmail.com

[1] C.J. Pethick and H. Smith, *Bose-Einstein Condensation in Dilute Gases* (Cambridge University Press, Cambridge, 2008).
[2] L.P. Pitaevskii and S. Stringari, *Bose-Einstein Condensation* (Oxford University Press, Oxford, 2003).
[3] P.G. Kevrekidis, D.J. Frantzeskakis, and R. Carretero-González (eds.), *Emergent Nonlinear Phenomena in Bose-Einstein Condensates. Theory and Experiment* (Springer-Verlag, Berlin, 2008).
[4] P.G. Saffman, *Vortex Dynamics* (Cambridge University Press, Cambridge, 1992).
[5] L.M. Pismen, *Vortices in Nonlinear Fields* (Clarendon, Oxford, 1999).
[6] S. Komineas, Eur. Phys. J.- Spec. Topics **147** 133 (2007).
[7] P.G. Kevrekidis, D.J. Frantzeskakis, and R. Carretero-González, *The defocusing nonlinear Schrödinger equation: from dark solitons, to vortices and vortex rings* (SIAM, Philadelphia, 2015).
[8] A.L. Fetter and A.A. Svidzinsky, J. Phys.: Condens. Matter **13**, R135 (2001).
[9] A.L. Fetter, Rev. Mod. Phys. **81**, 647 (2009).
[10] D.V. Freilich, D.M. Bianchi, A.M. Kaufman, T.K. Langin, and D.S. Hall, Science **329**, 1182 (2010).
[11] J. Ruostekoski and J.R. Anglin, Phys. Rev. Lett. **86**, 3934–3937 (2001).
[12] C.M. Savage and J. Ruostekoski Phys. Rev. Lett. **91**, 010403 (2003).
[13] J.Y. Choi, W.J. Kwon and Y.I. Shin, Phys. Rev. Lett. **108**, 035301 (2012).
[14] L.S. Leslie, A. Hansen, K.C. Wright, B.M. Deutsch, and N.P. Bigelow, Phys. Rev. Lett. **103**, 250401 (2009).
[15] J. Lovegrove, M.O. Borgh, and J. Ruostekoski, Phys. Rev. Lett. **112**, 075301 (2014).
[16] Y.V. Kartashov, B.A. Malomed, Y. Shnir, and L. Torner Phys. Rev. Lett. **113**, 264101 (2014).
[17] Y.M. Bidasyuk, A.M. Chumachenko, O.O. Prikhodko, S.I. Vilchinskii, M. Weyrauch, A.I. Yakimenko, arXiv:1508.01697.
[18] R.N. Bisset, W. Wang, C. Ticknor, R. Carretero-González, D.J. Frantzeskakis, L.A. Collins, and P.G. Kevrekidis, Phys. Rev. A **92**, 043601 (2015).
[19] A.A. Svidzinsky and A.L. Fetter, Phys. Rev. A **62**, 063617 (2000).
[20] P. H. Roberts and J. Grant, J. Phys. A: Gen. Phys. **4**, 55–72 (1971).
[21] T.-L. Horng, S.-C. Gou, and T.-C. Lin, Phys. Rev. A **74**, 041603 (2006).
[22] G. Theocharis, D.J. Frantzeskakis, P.G. Kevrekidis, B.A. Malomed, and Yu.S. Kivshar, Phys. Rev. Lett. **90**, 120403 (2003).
[23] A.M. Kamchatnov and S.V. Korneev, Phys. Lett. A **374**, 4625 (2010).
[24] B. Jackson, J.F. McCann, and C.S. Adams, Phys. Rev. A **61**, 013604 (1999).
[25] C.T. Kelly, Solving Nonlinear Equations with Newton's Method, (SIAM, Philadelphia, 2003).
[26] S. Ronen, D.C.E. Bortolotti, and J.L. Bohn, Phys. Rev. A **74**, 013623 (2006).
[27] P.B. Blakie, D. Baillie, and R.N. Bisset, Phys. Rev. A **86**, 021604(R) (2012).
[28] R.J. Dodd, K. Burnett, Mark Edwards, and Charles W. Clark, Phys. Rev. A **56**, 587 (1997).
[29] Barry I. Schneider, Lee A. Collins, and S.X. Hu, Phys. Rev. E **73**, 036708 (2006).
[30] S. Stringari. Phys. Rev. Lett. **77**, 2360 (1996).
[31] A.J. Allen, S. Zuccher, M. Caliari, N.P. Proukakis, N.G. Parker, and C.F. Barenghi, Phys. Rev. A **90**, 013601 (2014).
[32] T. Wells, A.U.J. Lode, V.S. Bagnato, M.C. Tsatsos, J. Low Temp. Phys. **180**, 133 (2015).
[33] N.P. Proukakis, B. Jackson, J. Phys. B **41**, 203002 (2008).
[34] I. Carusotto and C. Ciuti, Rev. Mod. Phys. **85**, 299

(2013).
[35] We invite the interested reader to see the corresponding movies for the dynamics at this address: http://nonlinear.sdsu.edu/∼carreter/Hopfion.html

SUPPLEMENTAL MATERIAL:

Robust Vortex Lines, Vortex Rings and Hopfions in 3D Bose-Einstein Condensates

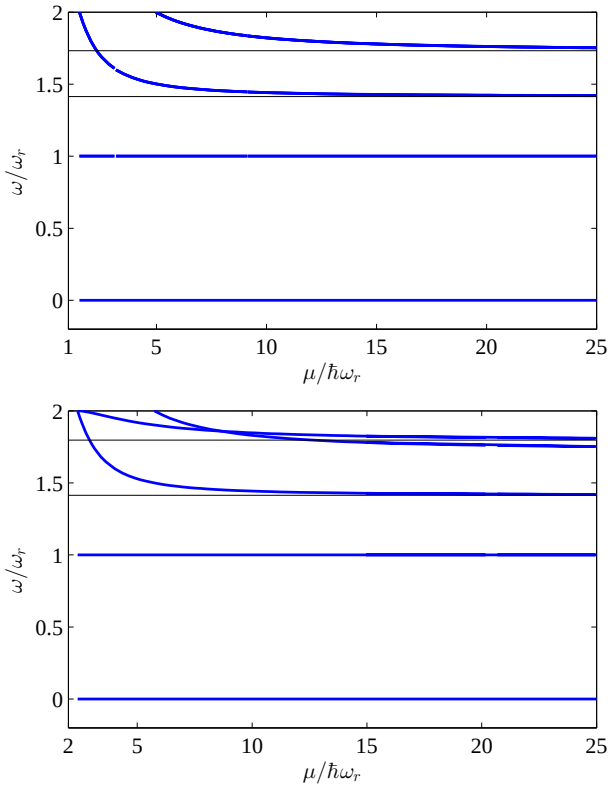

FIG. 5: (Color online) BdG-frequency spectrum for the ground state (bearing no vorticity) when $\omega_z/\omega_r = 1$ (top panel) and $\omega_z/\omega_r = 2.8$ (bottom panel). Stable (real) components are depicted by the thick (blue) lines. There are no unstable (imaginary) eigenvalues for the ground state. The thin horizontal lines pertain to the TF analytical predictions of Ref. [30].

Figure 5 depicts the BdG spectrum for the ground state of the system, i.e., in the absence of any coherent structure, starting from the linear limit and continuing all the way to the large μ, so-called Thomas-Fermi (TF) limit. The top panel depicts the spectrum for an isotropic trap ($\omega_z/\omega_r = 1$) while the bottom panel corresponds to an oblate trap ($\omega_z/\omega_r = 2.8$). The thick (blue) lines correspond to the numerical results, while the thin horizontal (black) lines correspond to the first few collective mode excitations predicted by the theory [30]. It is

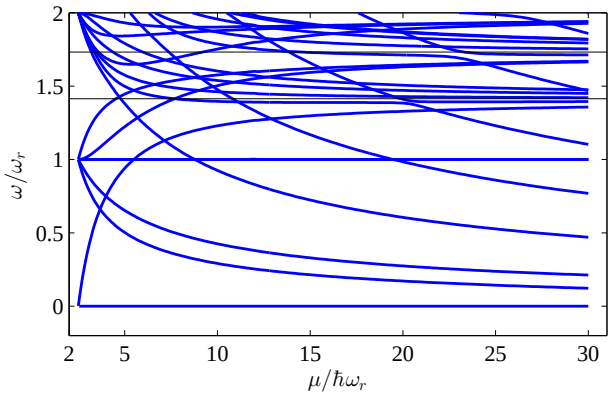

FIG. 6: (Color online) BdG-frequency spectrum for the vortex line when $\omega_z/\omega_r = 1$. Stable (real) components are depicted by the thick (blue) lines. There are no unstable (imaginary) eigenvalues for this case. The thin horizontal lines pertain to the TF analytical predictions of Ref. [30] for the ground state modes.

clear that, as the chemical potential μ increases, corresponding to a higher number of atoms in the condensate, the full numerical spectrum coincides with the collective excitations prescribed by the theory.

Figure 6 depicts the BdG spectrum for the vortex line (VL) in an isotopic trap ($\omega_z/\omega_r = 1$). Notice that modes corresponding to the ground state (see Fig. 5) are also contained in the spectrum of the VL and, as μ increases, one recovers again the collective excitations prescribed by the theory [30]. In a similar manner as the spectrum for the VL contains the spectrum of the background cloud, the modes corresponding to: (i) the collective excitations of the background cloud (see Fig. 5), (ii) the VL (see Fig. 6), and (iii) the VR (see Fig. 1 in the main text) are "inherited" by the hopfion as it may be noted in Fig. 2 of the main text.

Finally, in Fig. 7 we depict the evolution of the unstable dynamics for the $n = 3$ undulation mode of a VR in an oblate trap ($\omega_z/\omega_r = 2.8$). The dynamics is similar as the one observed for the unstable evolution of the $n = 2$ mode in Fig. 3 of the main text. However, in this case, owing to the higher undulation number of the unstable mode, the dynamics is more complex and involves the breakup of the VR into six filaments (non-straight VLs) traversing the BEC cloud. These filaments in turn interact and reconnect forming other (smaller) VRs that in turn evolve and interact with the other filaments. To see movies corresponding to the destabilization of (a) the VR along the $n = 2$ mode [Movie#1], (b) the VR along the $n = 3$ mode [Movie#2], and (c) the hopfion [Movie#3], please see Ref. [35].

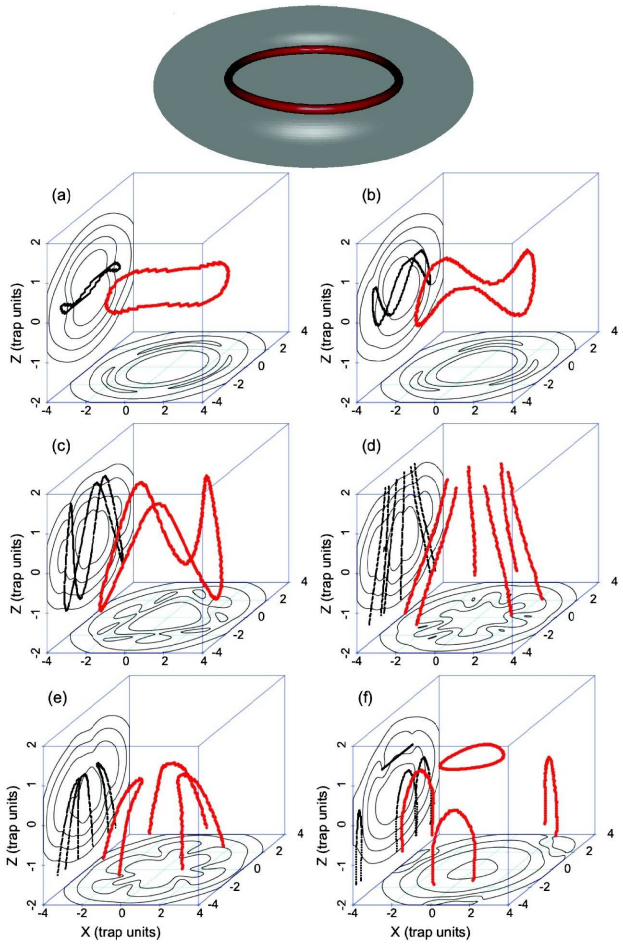

FIG. 7: (Color online) Dynamics of the VR, demonstrating instability to an $n = 3$ undulation, shown at times $t/\omega_r = 0$ (a), 4.9 (b), 7.4 (c), 8.4 (d), 9.4 (e) and 11.6 (f). Parameters: $\omega_z/\omega_r = 2.8$ and $\mu \approx 15.3$. Red (gray) curves indicate vortex core positions; thick black lines show the vortex core projections onto the (y, z) plane; thin-black contour lines represent the column density projections at 0.2, 0.4, 0.6 and 0.8 of the peak. Top: iso-density surface of the stationary state at 0.1 of the peak; the inner iso-density surface, due to the core, is colored red. To see a movie of the dynamics see Ref. [35] [Movie#2].